Search for WIMP Inelastic Scattering Off Xenon Nuclei With XENON100 Data

(The XENON100 Collaboration)

(Dated: January 19, 2017)

Some nice abstract here.....

I. INTRODUCTION

Astrophysical and cosmological evidence indicates that the dominant mass fraction of our Universe consists of some yet unknown form of dark, or invisible matter. The dark matter could be made of new, stable or long-lived and yet undiscovered particles. Well-motivated theoretical models going beyond the Standard Model of particle physics predict the existence of Weakly Interacting Massive Particles (WIMPs), which are natural candidates for dark matter. This hypothesis is currently being tested by several direct and indirect detection experiments, as well as at the LHC [1, 2].

Most direct detection searches focus on elastic scattering of galactic dark matter particles off nuclei, where the keV-scale nuclear recoil energy is to be detected [3–5]. In this work, the alternative process of inelastic scattering is explored, where a WIMP-nucleus scattering induces a transition to a low-lying excited nuclear state. The experimental signature is a nuclear recoil detected together with the prompt de-excitation photon [6].

We consider the ^{129}Xe isotope, which has an abundance of 26.4% in natural xenon, and a lowest-lying $3/2^+$ state at 36.6 keV above the $1/2^+$ gound state. The electromnagnetic nuclear decay has a half-life of 0.97 s. The signatures of inelastic scattering in xenon have been studied in detail in [7]. It was found that this channel is complementary to spin-dependent, elastic scattering, dominating the integrated rates above $\simeq 10\,\mathrm{keV}$ energy depositions. In addition, in case of a positive signal, the observation of inelastic scattering would provide a clear indication of the spin-dependent nature of the fundamental interaction.

Our paper is structures as follows. In Section II we briefly describe the XENON100 detector and the employed data set in this analysis. In Section III we detail the data analysis method, including the simulation of the expected signal and the background model. We conclude in Section IV with our results and new constraints on inelastic WIMP-nucleus scatters.

II. THE XENON100 DETECTOR

The XENON100 experiment operates a dual-phase (liquid and gas) xenon time projection chamber (TPC) at the Laboratori Nazionali del Gran Sasso (LNGS) in Italy. It contains 161 kg of xenon in total, with 62 kg in the active region of the TPC. These are monitored by 242 1-inch square, low-radioactivity, UV-sensitive photomultiplier tubes (PMTs) arranged in two arrays, one in the liquid and one in the gas. The PMTs detect the prompt scintillation (S1) and the delayed, proportional scintillation signal (S2) created by a particle interacting in the active TPC region. The S2-signal is generated due to ionisation electrons, drifted in an electric field of 530 V/cm and extracted into the gas phase by a stronger field of $\sim 12\,\mathrm{kV/cm}$, where the proportional scintillation, or electroluminiscence, is produced. These photons carry the (x, y) information of the interaction site, while the $z-$information comes from the drift time measurement. The TPC thus yields a three-dimensional event localisation, with an (x, y) resolution of $<3\,\mathrm{mm}$ $(1\,\sigma)$, and a z resolution of $<0.3\,\mathrm{mm}$ $(1\,\sigma)$, enabling to reject the majority of background events via fiducial volume cuts [8]. The ratio S2/S1 provides the basis for distinguishing between nuclear recoils (NRs), as induced by fast neutrons and expected from elastic WIMP-nucleus scatters, and electronic recoils (ERs) produced by β and γ-rays.

XENON100 has acquired science data between 2008-2015, and has set competitive constraints on spin-independent [9, 10] and spin-dependent [10, 11] elastic WIMP-nucleus scatters, on solar axions and galactic ALPs [12], as well as on leptophilic dark matter models [13–15].

Here we explore a potential new signature in the XENON100 detector, caused by spin-dependent, inelastic WIMP-^{129}Xe scatters. The expected inelastic scattering signature is a combination of an ER and a NR, due to the short lifetime of the excited nuclear state and the short mean free path of $\sim$0.15 mm of the 39.6 keV de-excitation photon.

III. DATA ANALYSIS

This analysis is performed using XENON100 Run-II science data, which corresponds to a data set with an exposure of 224.6 live days. The detector response to ERs has been characterised with ^{60}Co and ^{232}Th calibration sources, while the response to NRs was calibrated with an ^{241}AmBe (α, n)-source. This fast neutron source gives rise to elastic and inelastic neutron-nucleus scatters, and can thus be employed to define the expected signal region for inelastic WIMP-nucleus scatters.

A. Signal Correction

A particle interaction in the liquid xenon produces an S1 and a correlated S2 signal with a certain number of photoelectrons (PE) observed by the PMTs. The non-uniform scintillation light collection by the PMT arrays, due to solid angle effects, Rayleigh scattering length, reflectivity, transmission of the electrodes, etc, lead to a position-dependent S1 signal. The warping of the top meshes (inducing a variation in the width of the gas gap between the anode and the liquid-gas interface), the absorption of electrons by residual impurities as they drift towards the gas region, as well as solid angle effects lead to a position-dependent S2 signal. These signals are thus corrected in 3 dimensions, using various calibration data, as detailed in [8, 16], with the corrected quantities denoted as cS1 and cS2, and defined in [16]. The trigger efficiency in this run was 100% for S2>300 PE.

B. Signal Region and Event Selection

As explained in Section I, the inelastic scattering of a WIMP with a ^{129}Xe nucleus produces an energy deposit via a NR with subsequent emission of a 39.6 keV de-excitation photon. The largest fraction of the energy released in the event is via an ER, due to the emitted photon which loses its energy in the LXe. This represents an unusual signature compared to the one expected from an elastic scatter, and brings the signal region to overlap with the ER background region. The selected region of interest (ROI) for this analysis surrounds the 39.6 keV xenon line in the cS1-cS2 plane and is further divided into sub-regions, as shown in Figures 1 and 2. These sub-regions were defined such as to contain roughly a similar number of expected background events in each region. The control regions CR1 and CR2 are chosen to be as close as possible to the signal regions, and are used as cross check of the background shape distribution.

Apart from the condition to occur in the defined region of interest in the cS2-cS1-plane, valid events are required to fulfil several selection criteria, which can be summarised as follows: basic data quality cuts, energy selection and S2 threshold cut, veto cut for events with energy release in the detector's active LXe shield, selection of single-scatter events and of a predefined fiducial volume.

This analysis closely follows the event selection criteria described in detail in [16] for Run-II, with only a few exceptions reported in what follows. The cut on the width of the S2 signal as a function of drift time (where the maximal drift time is 176 μs and the width values range from ∼1-2 μs) has been optimised on a sample of events selected from the 39.6 keV line and set to a 95% acceptance on these. This cut ensures that the S2-signal width is consistent with the z-position calculated from the observed time difference between the S1 and S1 signals. Events are required to be single-scatters by applying a threshold cut on the size of the second largest S2 peak. For this analysis, the threshold has been optimised to 160 PE and set constant as function of S2 signal size. Finally, the chosen fiducial volume corresponds to 34 kg of liquid xenon.

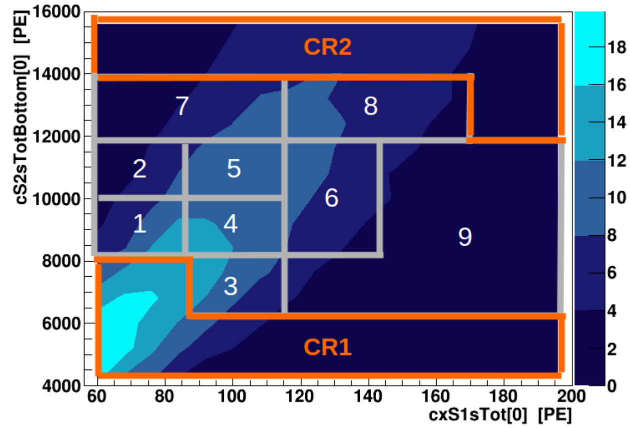

FIG. 1. Signal (1-9) and control (CR1 and CR2) regions for the inelastic WIMP-^{129}Xe interaction in the cS2 versus cS1 plane. Their definition is given in the text.

C. Signal Simulation

The detector response to inelastic WIMP-^{129}Xe interactions was simulated using an empirical signal model. The total deposited energy is divided into two independent contributions: one coming from the 39.6 keV de-excitation photon and the other from the simultaneous nuclear recoil of the xenon atom. The detected light (S1) and charge (S2) signals are simulated separately for each of the two contributions and then added together. This is due to the fact that the light and charge yields depend on the type of interaction (ER vs. NR), and on the deposited energy.

The distribution of an ER induced by the de-excitation photon in the cS1-cS2 plane is simulated assuming a two dimensional normal probability distribution function (pdf), $f(cS1_{er}, cS2_{er})$, described (apart from a constant normalisation factor) by the following equation:

$$f(cS1_{er}, cS2_{er}) = \exp\Big\{-\frac{1}{2(1-\rho^2)}\Big[\frac{(cS1_{er}-\mu_{cS1_{er}})^2}{\sigma_{cs1}^2} + \frac{(cS2_{er}-\mu_{cS2_{er}})^2}{\sigma_{cs2}^2} - \frac{2\rho\cdot(cS1_{er}-\mu_{cs1})(cS2_{er}-\mu_{cs2})}{\sigma_{cs1}\sigma_{cs2}}\Big]\Big\} \tag{1}$$

where μ_{cS1} and μ_{cS2} represent the average observed $cS1_{er}$ and $cS2_{er}$ signals given a 39.6 keV ER, σ_{cs1} and σ_{cs2} are the standard deviation in $cS1_{er}$ and $cS2_{er}$ respectively, while ρ stands for the correlation between the cS1 and cS2 signals. The detector-related light yield L_y at 39.6 keV, necessary to evaluate the average number of prompt photons detected (μ_{cS1}), is obtained from the NEST model [17–19] fit to data collected with several γ-lines. The average light yield at 39.6 keV is 2.7 PE/keV.

The same model is used to predict the charge yield at 39.6 keV, which is afterwards scaled according to the detector's secondary scintillation gain Y. The latter is determined from detector's response to single electrons [20]. The energy resolution at 39.6 keV in cS1 and cS2 has been measured to be 15.8% and 14.7%, respectively, and is used to extract the standard deviations σ_{cs1}, σ_{cs2}. The correlation parameter is assumed to be independent of energy (at least in the considered narrow energy range) and measured using the 164 keV line from the decay of the ^{131m}Xe isomer ($T_{1/2}$=11.8 d) produced during the ^{124}AmBe run. This γ-line is chosen because it allows to disentangle efficiently the contribution from the nuclear recoil. The measured correlation coefficient is $\rho = -0.45 \pm 0.10$.

The cS1 and cS2 distributions from the NR contribution are predicted starting from the expected nuclear recoil energy spectrum of WIMP inelastic interactions [7]. The average cS1 and cS2 are given by equations 2 and 3 respectively, where $\mathcal{L}_{eff}$ is the liquid xenon relative scintillation efficiency for NRs, while $S_{ee} = 0.58$ and $S_{nr} = 0.95$ describe the scintillation quenching of ER and NRs, respectively, due to the electric field [21]. The parameterisation and uncertainties of $\mathcal{L}_{eff}$ as a function of nuclear recoil energy E_{nr} are based on existing direct measurements [22]. The light yield for 122 keV ERs is taken from the same NEST model fit as described above. For cS2, the parameterisation of $Q_Y(E_{nr})$ is taken from [23]. Finally, all detector related resolution effects are introduced following the prescriptions described in [16].

$$cS1_{nr} = E_{nr}\,\mathcal{L}_{eff}(E_{nr})\,L_y\,\frac{S_{nr}}{S_{ee}} \qquad (2)$$

$$cS2_{nr} = E_{nr}\,Q_Y(E_{nr})\,Y \qquad (3)$$

The pdf of the ER and NR contributions are then convoluted together to obtain the overall pdf of the expected signal. A 2D (cS1 versus cS2) acceptance map is applied to the signal pdf to reproduce data selection effects. Acceptances are computed separately for each selection criteria using the ^{124}AmBe calibration sample. Other selections such as the liquid xenon veto cut, and the single-scatter interaction represent an exception and a dedicated computation has been performed in these cases. The combined acceptance of all selection criteria in the region of interest averages to $\sim(0.80 \pm 0.05)$. Figure 1 shows an example of fully simulated signal model for a WIMP mass of 100 GeV/c^2.

The signal simulation procedure has been validated by reproducing the 39.6 keV xenon line from interactions due to neutrons from the ^{124}AmBe source and comparison to data. For this comparison, the proper ^{124}AmBe nuclear recoil and acceptances were simulated. The simulated events were in agreement with calibration data within statistical uncertainties. Should we show an example, namely a figure from the signal model note?

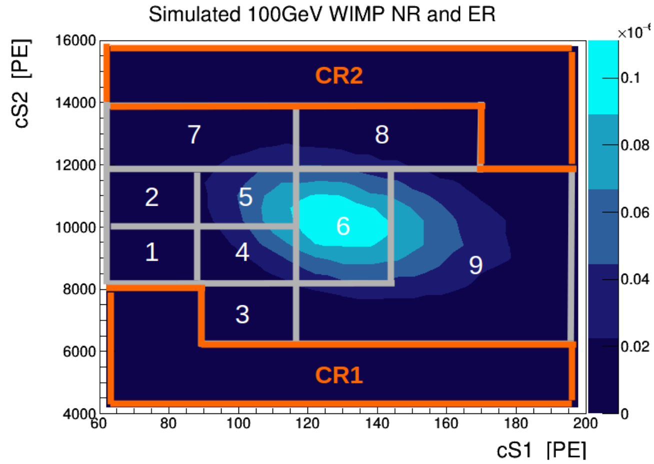

FIG. 2. Simulated signal (1-9) and control (CR1 and CR2) regions for a WIMP mass 100 GeV/c^2.

D. Background Model

The background in the region of interest for inelastic scattering is dominated by ERs due the residual radioactivity of detector materials, due to ^{85}Kr present in the liquid xenon ($\sim$55%) as well as due to ^{222}Rn decays in the liquid (<7%) [24]. The background contribution from inelastic scatters of radiogenic or cosmogenic neutrons (producing a 39.6 keV de-excitation line) is negligible thanks to the very low expected neutron scattering rate in the detector [25].

The expected background is modelled using data from the ^{60}Co calibration campaign, which are assumed to well represent the background density distribution in the cS1-cS2 plane. The calibration sample yields about 2.2×10^4 events in the ROI; these are then scaled to the science data according to a measured scale factor τ_{bkg}. This scale factor, which is merely the ratio between the data and calibration sample yields, is measured in the two control regions shown in Figure 1 and labelled CR1 and CR2. The two control regions give compatible results and the computed average is $\tau_{bkg} = 0.034 \pm 0.002$, where the reported uncertainty is of statistical nature only.

The distribution of the calibration sample has been compared to the data of the science run in the two control regions, and agreement was found within statistical uncertainties. Furthermore, ^{60}Co calibration data have been compared in the region of interest to data from the ^{232}Th calibration campaign, and the largest deviation between the two shapes is within 4%. An additional systematic uncertainty of 4% has thus been applied to the expected background yield of each sub-region of the ROI. Should we show a figure, namely the agreement of data and BG model for the control regions? Like the second figure in the background model check note.

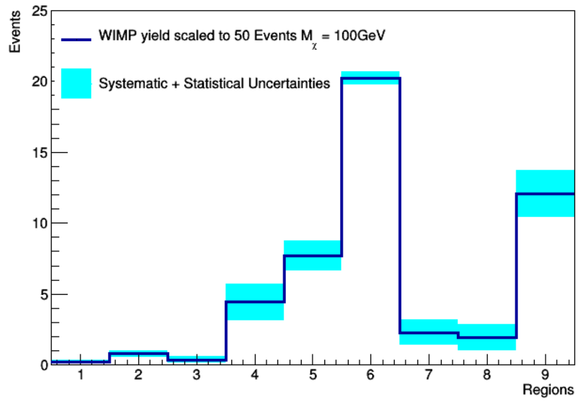

FIG. 3. Predicted signal (blue curve), along with statistical and systematic uncertainties (cyan region) simulated for a WIMP mass of 100 GeV/c^2. The signal and its uncertainties are shown as a function of the signal region number Maybe there is a better way to say this, or leave out?. The signal has been scaled for a total number of 50 events.

E. Systematic Uncertainties

Uncertainties on the prediction of the total number of background events arise from the uncertainty on the measurement of the normalisation factor, τ_{bkg}, and amount to 6%. Systematic uncertainty on the shape of the predicted background distribution are assessed by the maximal observed discrepancy in the ROI between the ^{60}Co and ^{232}Th calibration samples. As explained, a 4% systematic uncertainty is added to the expected yield of each sub-region. Uncertainties belonging to different sub-regions in the ROI are considered independent from one another.

Uncertainties on the total yield of signal events arising from selections acceptance uncertainties are found to be very weakly dependent on the WIMP mass, and an overall 6% acceptance uncertainty is applied to all WIMP hypotheses.

Uncertainties on the energy scale and, more generally, related to detector responses are parameterised using the respective uncertainties on the measures of L_y, $\mathcal{L}_{eff}$, Y, Q_Y and ρ. The simulation shows that these uncertainties mainly affect the pdf of the signal model in the ROI, and very weakly the total signal yield. They are taken into account by simulating several signal pseudo-samples for each WIMP mass, where the pseudo-samples are produced by varying the model parameters within their ±1 standard deviations. For each sub-region an overall uncertainty is then computed, by adding in quadrature the variations of each pseudo-sample with respect to nominal. Figure 3 shows an example of such a systematic uncertainty computation for a WIMP mass of 100 GeV/c^2.

All the uncertainties discussed here are parameterised with a binned profile likelihood function using the framework from [26, 27]. All the parameters related to systematic uncertainties are assumed to be normally distributed.

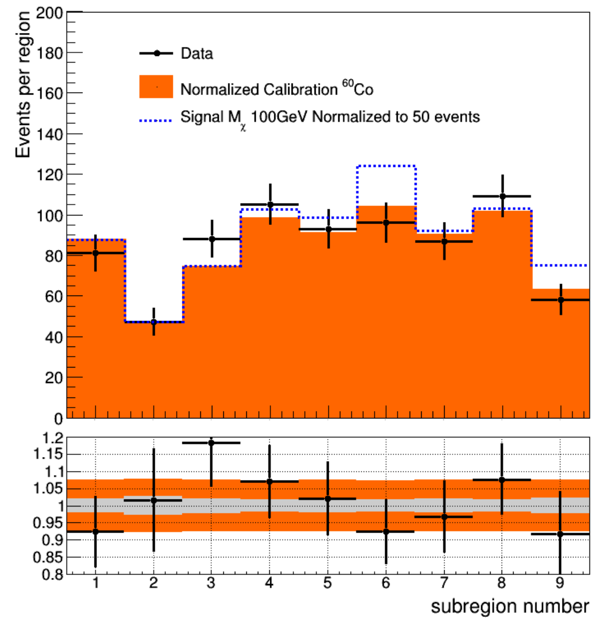

FIG. 4. Distribution of observed events in the region of interest (data points), along with the normalised distribution from calibration data (filled histogram). The bottom panel displays the ratio between data and expected background, where the grey and orange shaded areas represent the statistical and systematic uncertainty on the background expectation, respectively. The expected signal for a WIMP mass of 100 GeV/c^2 (blue dashed), and normalised to a total of 50 events, is also shown.

IV. RESULTS AND DISCUSSION

Using a fiducial volume containing 34 kg of liquid xenon and 224.6 live days of data yields 764 events observed in the region of interest. This number is compatible with the expectation of 756 $\pm$ 5 (stat) $\pm$ 55 (syst) events from the background only hypothesis. Figure 4 shows the distribution of events in the region of interest, where the bottom panel displays the ratio between data and expected background. The grey and orange shaded areas represent the statistical and systematic uncertainty on the background expectation, respectively. The expected signal for a WIMP mass of 100 GeV/c^2, and normalised to a total of 50 events, is also shown.

This result is interpreted via a binned profiled likelihood approach by means of the test statistic $\tilde{q}$ and its asymptotic distributions, as described in [28]. Assuming an isothermal WIMP halo with a local density of ρ_χ = 0.3 GeV/cm^3, a local circular velocity of v_0 = 220 km/s, and a galactic escape velocity of $v_{\rm esc}$ = 544 km/s, other assumptions..., a 90% CL$_s$ [29] confidence level upper limit on the spin-dependent inelastic WIMP-nucleon cross section as a function of WIMP mass is computed. We employ the nuclear structure factors as calculated in [35], based on state-of-the-art large-scale shell-model calculations, with chiral effective field theory WIMP-nucleon currents.

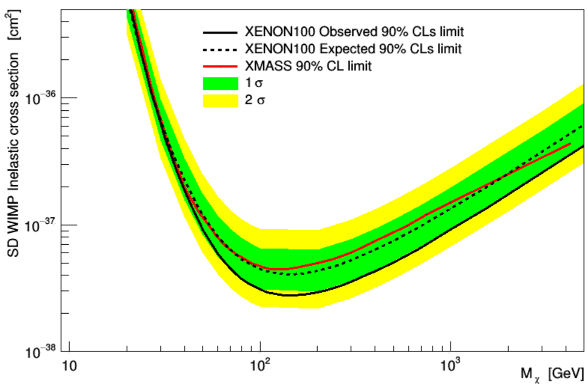

FIG. 5. Upper limit (black curve) on the spin-dependent, inelastic WIMP-nucleon cross section as a function of WIMP mass. The expected median sensitivity (dashed curve) along with the relative one (green area) and two (yellow area) standard deviation uncertainty is also shown. This result is compared to the upper limit (at 90% C.L.) obtained by the XMASS experiment (red curve) [30].

Our result is shown in Figure 5, together with the expected median sensitivity and its relative one and two standard deviation uncertainty. The most constraining upper limit is $3.3 \times 10^{-38}\,\mathrm{cm}^2$ (at 90% CL_s confidence level) is for a WIMP of mass $100\,\mathrm{GeV/c}^2$.

This results is compared to the one obtained by the XMASS experiment [30], a single phase liquid xenon detector, which used a fiducial volume containing 41 kg of LXe and 165.9 live days of data. Decide which other experiment to also plot - DAMA LXe? However only XMASS uses the same form factors as we do.

Our limit improves upon the XMASS result and constrains new parameter space for the spin-dependent, inelastic scattering cross section. While these upper limits are not competitive to spin-dependent, elastic scattering results, as obtained by XENON100 [11] and LUX [31] (with a cross section minimum of $\sim 2 \times 10^{-40}\,\mathrm{cm}^2$, at 90% C.L., for a $100\,\mathrm{GeV/cm}^2$ WIMP), our results set the pathway for a sensitive search of inelastic WIMP-nucleus scattering in running or upcoming liquid xenon experiments such as XENON1T [32], XENONnT [32], LZ [33], and DARWIN [34]. In these larger detectors, with lower intrinsic backgrounds from ^{85}Kr and ^{222}Rn decays, and improved self-shielding, the electronic recoil background will be reduced by a few orders of magnitude with respect to XENON100, and ultimately dominated by solar neutrino interactions [35].

The discovery of this interaction channel would be a clear signature for a spin-dependent nature of the interaction, and would provide a potential handle to constrain the WIMP mass [7].

[1] J. Silk et al. *Particle Dark Matter: Observations, Models and Searches.* 2010.

[2] Laura Baudis. Dark matter detection. *J. Phys.*, G43(4):044001, 2016.

[3] Laura Baudis. Direct dark matter detection: the next decade. *Phys. Dark Univ.*, 1:94, 2012.

[4] Laura Baudis. Dark matter searches. *Annalen Phys.*, 528:74, 2016.

[5] Teresa Marrodan Undagoitia and Ludwig Rauch. Dark matter direct-detection experiments. *J. Phys.*, G43(1):013001, 2016.

[6] John R. Ellis, R. A. Flores, and J. D. Lewin. Rates for Inelastic Nuclear Excitation by Dark Matter Particles. *Phys. Lett.*, B212:375–380, 1988.

[7] L. Baudis, G. Kessler, P. Klos, R. F. Lang, J. Menendez, S. Reichard, and A. Schwenk. Signatures of Dark Matter Scattering Inelastically Off Nuclei. *Phys. Rev.*, D88(11):115014, 2013.

[8] et al Aprile E. The XENON100 Dark Matter Experiment. *Astropart. Phys.*, 35:573–590, 2012.

[9] E. Aprile et al. Dark Matter Results from 225 Live Days of XENON100 Data. *Phys. Rev. Lett.*, 109:181301, 2012.

[10] E. Aprile et al. XENON100 Dark Matter Results from a Combination of 477 Live Days. *Phys. Rev.*, D94(12):122001, 2016.

[11] E. Aprile et al. Limits on spin-dependent WIMP-nucleon cross sections from 225 live days of XENON100 data. *Phys. Rev. Lett.*, 111(2):021301, 2013.

[12] E. Aprile et al. First Axion Results from the XENON100 Experiment. *Phys. Rev.*, D90:062009, 2014.

[13] E. Aprile et al. Exclusion of Leptophilic Dark Matter Models using XENON100 Electronic Recoil Data. *Science*, 349(6250):851–854, 2015.

[14] E. Aprile et al. Search for Event Rate Modulation in XENON100 Electronic Recoil Data. *Phys. Rev. Lett.*, 115(9):091302, 2015.

[15] E. Aprile et al. Search for Electronic Recoil Event Rate Modulation with 4 Years of XENON100 Data. 2017.

[16] E. Aprile et al. Analysis of the XENON100 Dark Matter Search Data. *Astropart. Phys.*, 54:11–24, 2014.

[17] M Szydagis, A Fyhrie, D Thorngren, and M Tripathi. Enhancement of nest capabilities for simulating low-energy recoils in liquid xenon. *Journal of Instrumentation*, 8(10):C10003, 2013.

[18] John Allison et al. Geant4 developments and applications. *IEEE Trans. Nucl. Sci.*, 53:270, 2006.

[19] S. Agostinelli et al. GEANT4: A Simulation toolkit. *Nucl. Instrum. Meth.*, A506:250–303, 2003.

[20] E Aprile et al. Observation and applications of single-electron charge signals in the xenon100 experiment. *Journal of Physics G: Nuclear and Particle Physics*, 41(3):035201, 2014.

[21] E. Aprile, C. E. Dahl, L. DeViveiros, R. Gaitskell, K. L. Giboni, J. Kwong, P. Majewski, Kaixuan Ni, T. Shutt,

and M. Yamashita. Simultaneous measurement of ionization and scintillation from nuclear recoils in liquid xenon as target for a dark matter experiment. *Phys. Rev. Lett.*, 97:081302, 2006.

[22] E. Aprile et al. Dark Matter Results from 100 Live Days of XENON100 Data. *Phys. Rev. Lett.*, 107:131302, 2011.

[23] E. Aprile et al. Response of the XENON100 Dark Matter Detector to Nuclear Recoils. *Phys. Rev.*, D88:012006, 2013.

[24] E. Aprile et al. Study of the electromagnetic background in the XENON100 experiment. *Phys. Rev.*, D83:082001, 2011. [Erratum: Phys. Rev.D85,029904(2012)].

[25] E. Aprile et al. The neutron background of the XENON100 dark matter search experiment. *J. Phys.*, G40:115201, 2013.

[26] Lorenzo Moneta, Kevin Belasco, Kyle S. Cranmer, S. Kreiss, Alfio Lazzaro, Danilo Piparo, Gregory Schott, Wouter Verkerke, and Matthias Wolf. The RooStats Project. *PoS*, ACAT2010:057, 2010.

[27] Wouter Verkerke and David P. Kirkby. The RooFit toolkit for data modeling. *eConf*, C0303241:MOLT007, 2003. [,186(2003)].

[28] Glen Cowan, Kyle Cranmer, Eilam Gross, and Ofer Vitells. Asymptotic formulae for likelihood-based tests of new physics. *Eur. Phys. J.*, C71:1554, 2011. [Erratum: Eur. Phys. J.C73,2501(2013)].

[29] Alexander L. Read. Modified frequentist analysis of search results (The CL(s) method). In *Workshop on confidence limits, CERN, Geneva, Switzerland, 17-18 Jan 2000: Proceedings*, pages 81–101, 2000.

[30] H. Uchida et al. Search for inelastic WIMP nucleus scattering on ^{129}Xe in data from the XMASS-I experiment. *PTEP*, 2014(6):063C01, 2014.

[31] D. S. Akerib et al. Results on the Spin-Dependent Scattering of Weakly Interacting Massive Particles on Nucleons from the Run 3 Data of the LUX Experiment. *Phys. Rev. Lett.*, 116(16):161302, 2016.

[32] E. Aprile et al. Physics reach of the XENON1T dark matter experiment. *JCAP*, 1604(04):027, 2016.

[33] D. S. Akerib et al. LUX-ZEPLIN (LZ) Conceptual Design Report. 2015.

[34] J. Aalbers et al. DARWIN: towards the ultimate dark matter detector. *JCAP*, 1611(11):017, 2016.

[35] L. Baudis, A. Ferella, A. Kish, A. Manalaysay, T. Marrodan Undagoitia, and M. Schumann. Neutrino physics with multi-ton scale liquid xenon detectors. *JCAP*, 1401:044, 2014.